Beyond the Active Site: The addition of a remote loop reveals a new complex biological function for chitinase enzymes.

Dan Kozome[1], Adnan Sljoka[2,3], Paola Laurino[1]*

[1] Protein Engineering and Evolution Unit, Okinawa Institute of Science and Technology Graduate University (OIST), Okinawa 904-0495, Japan.

[2] Center for Advanced Intelligence Project, RIKEN, Tokyo 103-0027, Japan

[3] Department of Chemistry, York University, Toronto, ON M3J 1P3, Canada

Corresponding author: Paola Laurino

Email: paola.laurino@oist.jp

Abstract

Loops are small secondary structural elements that play a crucial role in the emergence of new enzyme functions. However, the evolutionary molecular mechanisms how proteins acquire these loop elements and obtain new function is poorly understood. To address this question, we studied glycoside hydrolase family 19 (GH19) chitinase - an essential enzyme family for pathogen degradation in plants. By revealing the evolutionary history and loops appearance of GH19 chitinase, we discovered that one loop which is remote from the catalytic site, is necessary to acquire the new antifungal activity. We demonstrated that this remote loop directly accesses the fungal cell wall, and surprisingly, it needs to adopt a defined structure supported by long-range intramolecular interactions to perform its function. Our findings prove that nature applies this new strategy at the molecular level to achieve a complex biological function while maintaining the original activity in the catalytic pocket, suggesting an alternative way to design new enzyme function.

Introduction

Protein evolution is an essential process that drives diversity in nature by enabling the emergence of new functions[1]. Understanding how protein evolves is fundamental, not only for unraveling the natural diversification of proteins but also for designing new protein functions *in vitro*. The structure of more than 30,000 proteins reveals that nature uses a limited number of basic structures (scaffolds) to achieve an enormous variety of functions[2]. Indeed, many reports demonstrate that this diversity is often acquired by diversifying the flexible catalytic loop structures exposed on the protein's surface, while preserving the robust scaffold and the active site residues common among the enzyme family as core structures[3–5]. For instance, altering catalytic specificity by grafting loop[6] or shaping the catalytic activity *via* mutations in the catalytic loop[7]. These strategies are a major source of structural and functional variation within protein superfamilies[8]. Thus, mutations in the catalytic loop regions have garnered significant attention because they can directly impact function. Indeed, because of their functional roles like ligand binding[9], promoting function via conformational changes[10], and functional switching[11], the propensity of loop regions to acquire mutations is evolutionarily advantageous. However, while previous studies have extensively explored the catalytic loops[6,71213] , the role of functional remote loop regions remains limited in functional switching or large conformational change allostery[14–16], especially, how new function is acquired *via* remote loop regions acquisitions / removals through evolution is poorly understood.

To understand how natural evolution acquires new functions *via* remote loops and its molecular mechanisms, we investigated the evolution of Glycoside Hydrolase family 19 chitinases (GH19 chitinase; EC 3.2.1.14). GH19 chitinase hydrolyzes the glycosidic bonds of chitin, namely beta-1, 4-linked *N*-acetyl-D-glucosamine. Chitin is the main component of

54 exoskeletons and cell walls of various organisms, including arthropods and fungi. Despite
55 lacking an endogenous substrate for plant chitinases, many plants synthesize various chitinases.
56 One of the physiological roles of chitinase is to defend plants against pathogenic fungi by
57 degrading chitin, a major component of the cell wall of many fungi[17]. Interestingly, even in
58 GH19 chitinases, some chitinases do not exhibit antifungal activity. Taira *et al.* reported a
59 difference in the antifungal activity of two chitinases from plants[18], - in this work, we will call
60 them loopless and loopful GH19 chitinases. Comparing the sequences and the structures of
61 both GH19, the catalytic residues and the core structure that consists of the catalytic cleft are
62 conserved. However, loopful GH19, a chitinase from rye seed, contains six loop regions,
63 whereas loopless GH19, a chitinase from moss, lacks five of those loop regions seen in loopful
64 GH19 (Fig. 1A and B). Interestingly, loopful GH19 exhibits antifungal activity against the
65 fungi *Trichoderma sp*., while loopless GH19 does not[18]. Mutational effects of insertion and
66 deletions (InDels) of these loop regions on catalytic activity or fold stability are previously
67 reported [19–23]. However, the molecular evolutionary basis for chitinase achieving an increase
68 in antifungal activity while seemingly having no impact on catalytic activity remains unclear.
69 Herein we investigated the evolution of GH19 chitinase to understand how functional
70 innovation occurred. We inferred five ancestral proteins with different loop combinations in
71 remote loop regions. By characterizing these proteins variants, we discovered that loop II is
72 critical for acquiring antifungal activity. Using structural analysis, molecular dynamics
73 simulations, and computational studies, we showed that this remote loop allows new function
74 through fine-tuned intramolecular interactions. Imaging studies via fluorescence microscope
75 experiments unraveled that the acquisition of remote loop II access the substrate in a new
76 specific cellular location, the fungal cell wall. This is the first report that highlights the
77 molecular evolutionary basis of how nature acquired remote loops in a protein structure to
78 access a new and complex biological function.

Results

Phylogenetic analysis reveals the emergence of antifungal activity in GH19 chitinase. To identify the remote loop regions acquisition that played a role in the emergence of antifungal activity and when such an acquisition occurred in GH19 chitinase, we performed phylogenetic analysis and ancestral sequence reconstruction. After extensive collection of all available sequences belonging to GH19 chitinase from plants and the removal of redundancy, we inferred the maximum-likelihood phylogenetic tree of 179 GH19 chitinase sequences. We used ancestral protein reconstruction to infer the most likely amino acid sequence for each ancestral node in the phylogeny. To avoid the bias that phylogenetic classification is affected by the presence or absence of loop regions, we inferred two phylogenetic trees using a multiple sequence alignment (MSA) of the collected sequences, and a MSA modified by removing the six loop regions in question. After we confirmed that the tree topology did not change based on the presence/absence of loop regions in the MSA (Fig. S2 and S3), we used the tree based on the unmodified MSA and selected five ancestral nodes where InDels of the loop regions occurred, designated Anc1 to Anc5 based on the presence/absence of loop regions in the extant sequences (Fig. 1C). We experimentally characterized chitinase activities and antifungal activities of five reconstructed ancestral proteins and two extant GH19 sequences. All five ancestral proteins showed a similar level of chitinase activity to the two modern GH19 chitinases (Table 1), while Anc5 also exhibited antifungal activity. Anc1-4 did not exhibit antifungal activity (Fig. 1D), suggesting that antifungal activity seems to be acquired during the transition from Anc4 to Anc5.

Characterization of the functional intermediates between Anc4 and Anc5. To identify the key loop insertion for antifungal activity acquisition, we constructed six variants of two

103 reconstructed ancestral proteins, Anc4 and Anc5 with different combinations of loop I and II
104 (Anc4 + Loop I, Anc4 + Loop II, Anc4 + Loop I and II, Anc5ΔLoop I, Anc5ΔLoop II, and
105 Anc5ΔLoop I and II). We experimentally characterized antifungal activities and hydrolytic
106 activities of these variants. To compare the strength of their antifungal activities, we calculated
107 IC_{50} by performing a hyphal re-extension inhibition assay. Addition/removal of loop I and/or
108 II regions did not affect their hydrolytic activities (1.1 – 1.5-fold) except for in the case of loop
109 I addition to Anc4. Insertion of loop I to Anc4 resulted in a loss of catalytic activity of Anc4
110 (Fig. 2B). However, removing loop II from Anc5 decreased its antifungal activity by 12-fold
111 while removing loop I did not influence its antifungal activity (roughly 1.02-fold increase, Fig.
112 2B). These results strongly suggest that loop II has a role in enhancing antifungal activity.
113 However, it is worth noting that the addition of loop II to Anc4 did not improve its antifungal
114 activity. Anc4 and 5 differ by 45 substitutions (Fig. 2A, C), suggesting that loop II enhances
115 antifungal activity in combination with residues in the protein scaffold.
116
117 **Structural analysis of Anc4 and Anc5 and molecular dynamics (MD) simulations revealed**
118 **the importance of long-range interactions in the emergence of antifungal activity.**
119 To get structural insights into the emergence of antifungal activity in GH19 chitinase, we first
120 solved the X-ray crystal structure of Anc4 and Anc5 (Table S4). Overall, the backbone
121 structures of Anc4 and Anc5 were nearly identical (RMSD of Cα = 0.478 Å) and the orientation
122 of catalytic residues is similar, suggesting that loop I and II addition/removal did not cause
123 major structural disruptions. This is supported by the fact that addition/removal of loop I and/or
124 II regions did not affect their hydrolytic activities except for the loop I insertion into Anc4 (Fig.
125 2B). The loss of the hydrolytic activity in Anc4 via loop I insertion might be due to the lack of
126 disulfide bonding between loop I and the core scaffold. This is because the cysteine residue

127 that forms the disulfide bonding with loop I is replaced by another residue (Val 81 in the MSA,
128 Fig. S5).
129 Although Anc4 and Anc5 showed no significant structural difference and their mutants Anc4
130 + Loop II and Anc5ΔLoop I had similar hydrolytic activity, their antifungal activities were
131 significantly different (Anc5ΔLoop I showed 56-fold higher activity than Anc4 + Loop II, Fig.
132 2B). Therefore, we explored the contributions of protein dynamics to the acquisition of
133 antifungal activity by performing molecular dynamics (MD) simulations. We performed four
134 runs of 200 ns simulations of the model structure of Anc4 + Loop II and Anc5ΔLoop I built
135 using Anc4 and Anc5 structures (PDB 8HNE and 8HNF). In Anc5ΔLoop I, the simulation
136 showed reduced mobility of the loop II regions and a loop region between the ninth and tenth
137 α-helices (positions 192 - 201) compared to Anc4 + Loop II (Fig. 3A, B). Some of the 45
138 substitutions support the stabilization of loop II in Anc5ΔLoop I. Structural comparison of
139 Anc4 and Anc5 revealed six substitutions forming new interactions with loop II regions (Fig.
140 3C). Two substitutions, p12K and n13H (small and large character indicates Anc4 and Anc5
141 state, respectively), formed new hydrogen bonding with Asp residue in loop II. The His 13
142 residue is also involved in hydrophobic interaction with Trp residue in loop II (Fig. 3C).
143 d197(217)R (residue numbers are responsible to Anc5ΔLoop I; residue numbers in Anc5 state
144 are in parentheses) substitution formed new hydrogen bonds between the N terminus and the
145 tenth α-helix (Fig. 3C). n193(213)G substitution reduced structural hindrance with the Tyr
146 residue in loop II (Fig. 3C). Loop II insertion into Anc4 caused a change in conformational
147 orientation of Ser 58, leading to a formation of a hydrogen bond between the oxygen atom of
148 Ser 58 and the nitrogen atom of the Gly 60 as seen between Thr 65 and Gly 67 in Anc5.
149 y194(214)F substitution reduced structural hindrance with the oxygen atom of Thr 65 (Fig. 3C).
150 These substitutions are important for stabilizing the loop II region to perform antifungal
151 activity. Furthermore, to investigate if the flexibility of the loop region between the ninth and

152 tenth α-helices (positions 192 - 201) affects the antifungal activity, we also constructed the
153 mutant of Anc5 and Anc5ΔLoop I that only disrupt the stability of this loop. MD simulations
154 and antifungal activity of these mutants revealed that the flexibility of a loop region between
155 the ninth and tenth α-helices (positions 192 - 201) did not contribute to enhance antifungal
156 activity (Figure S5 and TableS6).

157 To assess whether residues in the scaffold have long-range effects on rigidity and
158 conformational modifications of loop II, we utilized rigidity transmission allostery (RTA)
159 algorithms[24]. RTA is a computational approach based on mathematical rigidity theory[25,26] and
160 graph theory, which analyzes long-range communication and allosteric networks within protein
161 structures[27–30]. RTA measures whether local mechanical perturbation of rigidity at one site
162 propagates and modifies rigidity and conformational degrees of freedom at distant site(s) in
163 protein structure. Starting with a structure, RTA first utilizes the method Floppy Inclusion and
164 Rigid Substructure Topography (FIRST)[31] to generate a constraint network, where protein
165 structure is modeled in terms of vertices (atoms) and edges (i.e., covalent bonds, electrostatic
166 bonds, hydrogen bonds, and hydrophobic contacts). Every potential hydrogen bond is ranked
167 and assigned energy strength according to its donor-hydrogen-acceptor geometry. Upon
168 rigidification of individual site(s) (i.e. residues), RTA then quantifies transmission (changes)
169 of degrees of freedom and strength of communication across protein structure. RTA analysis
170 on Anc5ΔLoop I showed that several residues in the scaffold are involved in long-range
171 communication with loop II, revealing an allosteric network of residues that transmit
172 communication with loop II (Fig. 3D). Interestingly, many of the substitution residues are part
173 of this communication network, suggesting they impact the stability and conformational
174 dynamics of loop II. To further probe this, we applied FIRST and decomposed the protein
175 structures into rigid and flexible regions. FIRST rigid cluster decomposition on Anc4 + Loop
176 II and Anc5ΔLoop I structures predicted that loop II is stabilized by intra-hydrogen bonding

177 between the Pro 72 and the Asp 73 (residue number is based on the MSA in Fig. 2), which is
178 observed only in Anc5ΔLoop I structure (Fig. S6). This results in a strong rigid cluster in
179 Anc5ΔLoop I which persists over wide hydrogen bond energy strengths (Fig. S6).

180

181 **Loop II leads to gain of antifungal activity by promoting binding to the fungal cell wall.**
182 To understand the complex biological role of loop II, we performed fluorescence microscope
183 experiments. These experiments aimed at verifying if the acquisition of loop II in GH19
184 chitinase plays a role in binding to the surface of the fungal cell wall. For this purpose, we
185 prepared the catalytically inactive mutants of Anc4, Anc4 + Loop II, Anc5, Anc5ΔLoop I,
186 Anc5ΔLoop II, and Anc5ΔLoop I and II by replacing catalytic glutamate residue with
187 glutamine (The Glu 67 in the MSA, Fig. S2). This mutation makes proteins lose chitin
188 degrading activity in the fungal cell wall. These inactive mutants were tagged with
189 AlexaFluor488. By fluorescence microscope experiments, we observed that only Anc5 and
190 Anc5ΔLoop I bound to the surface of fungal hyphae (Figs. 4A and S7). This result is consistent
191 with the result that Anc5 and Anc5ΔLoop I showed 28-fold stronger antifungal activity than
192 Anc4 (Fig. 2B), suggesting that the acquisition of loop II is necessary to access the substrate in
193 the cell wall of fungi to perform antifungal activity. Surprisingly, Anc4+Loop II did not exhibit
194 any binding activity to the fungal cell wall, despite the presence of Trp residues (positions 68
195 and 78 in the MSA, Fig. 2B) known for their involvement in substrate binding interactions,[32]
196 as well as in stabilizing Loop II (Figs. 2B and 4A).[19] This result suggests that Loop II is
197 necessary to have a potential binding activity to fungal cell wall but requires the additional
198 substitutions to perform its binding activity.

199

200 **A gain of new function through a remote loop acquisition in combination with**
201 **substitutions.**
202 To investigate the contribution to the antifungal activity of the 45 substitutions, we constructed
203 mutants of Anc4+Loop II with substitutions in proximity to loop II. We chose six substitutions
204 within 4.0 Å from Loop II and introduced them accordingly to their proximity to each other's
205 (Fig. 4C: mutations A, p12K and n13H; mutation B, s58T mutations C, n193G, y194F, and
206 d197R). Mutations A, B, and C increased antifungal activity 4.7, 1.2, and 5.4-fold, respectively.
207 These substitutions increased antifungal activity while retaining the same degree of chitinase
208 activity (Table 2). Cell wall binding activity assay confirmed that integrating these mutations
209 increased binding activity to the fungal cell wall (Fig. 4D). MD simulations of these mutants
210 revealed a gradual reduction of loop II flexibility directly related to the introduction of these
211 six substitutions (Fig. 4F) Furthermore, these substitutions decreased only the mobility of loop
212 II not the one of a loop region between the ninth and tenth α-helices (positions 192 – 201, Fig.
213 S5). Furthermore, crystal structures of Anc4 + Loop II + A and Anc4+Loop II+A+B+C
214 revealed that their loop II structures are retained as in the structure of Anc5's loop II, namely
215 the antifungal active variant (Fig. S8) . Altogether, these results exemplifies that antifungal
216 activity enhanced by cell wall binding activity is supported by the substitutions that rigidify
217 loop II. This demonstrates the molecular evolution trajectory of acquiring a new functional
218 loop, wherein a distant loop is incorporated through Insertions and Deletions (InDels). This
219 process is further complemented by accumulated substitutions, leading to the protein gaining
220 a novel function.
221
222 **Discussion**
223

224 Proteins use the limited numbers of folds and have evolved their structure and function using
225 substitutions and insertions and deletions (InDels) of loops and other secondary structures[33,34].
226 However, most studies focused on substitutions and InDels are rarely considered. In these rare
227 cases, when InDels are studied, they consist of one to three amino acid removal or addition[35,36]
228 or graft of the catalytic loops[6,7,12]. Shining light on the roles of insertion or deletions of entire
229 remote loop regions in protein evolution can provide further understanding of how we can
230 engineer new protein functions. Our study reveals the molecular mechanism of an enzyme,
231 through addition of a remote loop, can acquire a new distinct function distant from the catalytic
232 site while maintaining its original activity.
233
234 To address this, we first identified the transition where the remote loop regions were inserted
235 or deleted during evolution of the enzyme. This is the first study, to our best knowledge, that
236 demonstrates that phylogenetic analysis and ancestral sequence reconstruction can explore
237 remote loop acquisition in enzymes and thus identify potential hotspots for loop engineering.
238 Most studies using ancestral sequence reconstruction have been performed with a fixed length
239 of multiple sequence alignment due to the ambiguous evolutionary information of InDels. In
240 our case, GH19 chitinases acquire an additional antifungal activity over original chitinase
241 activity, through InDels of remote loop regions. Our phylogenetic analysis with two multiple
242 sequence alignments (with/without the considered loop regions) showed that InDels of remote
243 loop regions did not occur frequently and the tree topology did not change significantly due to
244 the InDels of remote loop regions (Fig. S3). Thus, we identified the ancestral nodes where the
245 protein acquired/lost remote loops and inferred functional ancestral proteins with different loop
246 combinations (InDels). As previous studies[36–38] demonstrated that InDels in loop regions are
247 highly tolerated, our ancestral proteins showed robustness to add/remove loops. Thus, we
248 demonstrate that ancestral sequence reconstruction approach in enzyme family with structural

249 variations in loop regions is useful for designing enzyme with different loop combinations and
250 exploring the potential remote site for loop engineering.
251
252 Surprisingly these ancestral proteins have the same sequence length and almost
253 identical structure (RMSD of Cα = 0.478 Å), however, they showed significantly different
254 antifungal activity (Anc4 + Loop II and Anc5 ΔLoop I differ 40-fold in antifungal activity in
255 addition to 45 substitutions in the scaffold), indicating that structural dynamics play an
256 important role for the additional functions[39]. Our mutational analysis revealed that some of
257 substitutions are conserved in loopful-type GH19 chitinases (Fig. 4D) and six substitutions are
258 needed to perform new function (Figs. 4C and Table 2). In the evolution of GH19 chitinase,
259 loop insertion comes with stabilizing the key remote loop regions is important to perform new
260 protein functions, and this stabilization requires additional substitutions (Fig.4). By comparing
261 the evolutionary consequences of homologous proteins, researchers have discovered that loop
262 regions, or regions decorated by loops, govern protein dynamics to execute distinct functions
263 [3,40]. This characteristic can be harnessed through protein engineering to achieve functional
264 switches[2,6,14] . These significant mutational steps occur alongside substitutions in natural
265 sequences [41]. To date, no experimental work has demonstrated that such a dramatic functional
266 shift can be achieved remotely from the catalytic site. We unveiled the missing piece: a direct
267 evolutionary pathway for functional emergence involving the insertion of a crucial remote loop,
268 followed by subsequent substitutions that stabilize the dynamics of this critical loop.
269
270 In the evolution of GH19, it is interesting to note that the enzyme became dual-
271 functional with a new complex biological activity, accessing to the fungal cell wall while
272 maintaining its original activity even though a trade-off between the catalytic activities to
273 original substrate and the promiscuous substrate is often observed in protein evolution[42,43].

274 Trade-off can be associated with a change in the conformational dynamics of the catalytic
275 pocket optimizing to the substrate[39], and bifunctionality can be achieved when this trade-off is
276 weak enough to maintain original activity[44]. In the case of GH19, there is no significant change
277 in the dynamics near the catalytic residues due to the mutations and original catalytic activities
278 retained (Figs. 2B, 3A, and S5). The enzyme appears to possess an inherent conformer capable
279 of displaying antifungal activity, but this conformation is only accessible when the protein
280 interacts with the fungal cell wall, its substrate. The inserted remote loop played a pivotal role
281 in enabling remote functionality, thanks to complementary substitutions within the protein
282 scaffold. Thus, protein can acquire additional function while retaining its original catalytic
283 activity.
284
285 Strikingly, our findings show that the key loop insertion allowed the accessibility to the
286 substrate in a different cell types and cellular location (Fig. 4). Since the target substrate for
287 antifungal activity is located in the cell wall of fungi, not in the solution, the protein needs to
288 access the substrate location to perform protein function. The fluorescence labeling
289 experiments clearly show that chitinase access to the fungal cell wall to acquire antifungal
290 activity (Figs. 2B, 4, and S7). Nevertheless, the acquisition of this new and complex function
291 is possible only through the long-range interaction between the inserted secondary element and
292 the substituted residues in the protein scaffold (Figs. 3, 4, S5, and S8). Herein we are the first
293 to report how remote loop insertion plays an important role in accessing the substrate.
294
295 In addition, our findings are key to develop protein engineering methods aimed at accessing
296 water-insoluble substrates such as cellulose, chitin, and plastic. To achieve efficient
297 degradation of water-insoluble substrates, accessibility is equally important to catalytic
298 efficiency[45]. On the other hand, here, we are the first to prove how functional peptide grafting

299 is not only limited to catalytic loop, but it can be extended to remote loops. In conclusion, we
300 show an alternative and effective way to redesign or expand enzyme function, opening new
301 ways of thinking for enzyme designers.
302
303 **Methods**
304 *Phylogenetic analysis and ancestral sequence reconstruction*
305 2617 sequences of plant GH19 chitinase were collected from the UniProtKB database[46].
306 Redundant sequences with more than 50% sequence identity were filtered using the CD-HIT
307 program. The resulting 682 sequences were aligned using MAFFT ver. 7[47]. Only GH19
308 catalytic domain sequences were aligned, and additional domains were manually removed
309 using an alignment visualizing software, Aliview[48]. Sequences of a loopless type GH19
310 chitinase from *Gemmabryum coronatum* (Uniprot: A9ZSX9; residues 25-228) and a loopful
311 type GH19 chitinase from *Secale cereale* (Uniprot: Q9FRV0; residues 24-266) were used as
312 references for the smallest and largest GH19 catalytic domain, respectively. 11 bacterial GH19
313 chitinase sequences were added to the dataset as an outgroup. The resulting 179 sequences
314 were aligned with MAFFT and a maximum-likelihood phylogenetic tree was estimated using
315 the model (WAG+F+I+G4) automatically determined in IQ-TREE[49]. Ancestral protein
316 sequences were reconstructed using the empirical Bayesian method applied by IQ-TREE[49].
317 The ancestral sequences Anc1 to Anc5 were reconstructed using the WAG substitution matrix
318 together with the maximum-likelihood phylogenetic tree.
319
320 *Cloning and site-directed mutagenesis*
321 Codon-optimized genes encoding the ancestral GH19 chitinase proteins and loopful type GH19
322 chitinase from *Secale cereale* (Uniprot: Q9FRV0; residues 24-266) were synthesized by
323 TWIST Bioscience and cloned into the pET-22b (+) vector using the iVEC3[50]. PCR

324 amplifications for synthetic genes and a linear-pET-22b (+) vector were performed with using
325 PrimeSTAR® Max DNA polymerase (TaKaRa) and the designed primers (Supplementary
326 Table 1) containing appropriate overlapping regions for iVEC3. The gene coding loopless type
327 GH19 chitinase from *Gemmabryum coronatum* (Uniprot: A9ZSX9; residues 25-228) cloned
328 into the pET-22b (+) vector was a gift from Toki Taira.
329 Site-directed mutagenesis was achieved by Inverse PCR using PrimeSTAR® Max DNA
330 polymerase (TaKaRa) with the designed primers (Supplementary Table 1). Successful cloning
331 and mutagenesis were confirmed by Sanger sequencing.
332
333 *Protein expression and purification*
334 *E. coli* Shuffle T7 (DE3) cells harboring the protein gene of interest were grown in LB at 37 °C
335 to OD_{600} 0.6-0.8, induced with 0.1 mM β-d-1-isopropyl thiogalactopyranoside (IPTG) and
336 incubated further for 24 hours at 18 °C. Cells were pelleted and stored at −80 °C before protein
337 purification. The cells were disrupted by sonication in a 20 mM Tris-HCl buffer, pH 8.0. The
338 sonicated extract was separated into soluble and insoluble fractions by centrifugation at
339 12,000×g for 15 minutes at 4 °C. The soluble fraction was dialyzed against 10 mM sodium
340 acetate buffer, pH 5.0, and filtered before applying to a RESOURCE Q column (6 mL, Cytiva)
341 or HiTrap SP HP column (5 mL, Cytiva) previously equilibrated with the same buffer. The
342 elution was done with a linear gradient of NaCl from 0 to 0.3 M in the same buffer. The
343 recombinant protein fractions were collected and dialyzed against a 5 mM Tris-HCl buffer
344 containing 150 mM NaCl, pH 8.0. Purified recombinant proteins were concentrated using a
345 Millipore centrifugal protein concentration device (10 kDa cutoff) and loaded onto a
346 Superdex200 Hiload 16/600 column (Cytiva) equilibrated with 5 mM Tris-HCl buffer
347 containing 150 mM NaCl, pH 8.0. Protein purity was confirmed by SDS–PAGE, and protein

348 concentrations were measured spectrophotometrically using molar absorption coefficients
349 calculated in ProtParam (http://expasy.org/tools/protparam.html).
350
351 *Chitinase activity assay*
352 Chitinase activity was measured colorimetrically with glycol chitin as a substrate. Ten μL of
353 the sample solution was added to 150 μL of 0.2% (w/v) glycol chitin solution in 0.1 M sodium
354 acetate buffer, pH 5.0. After incubation of the reaction mixture at 37°C for 15 minutes, the
355 reducing power of the mixture was measured with ferric ferrocyanide reagent by Imoto &
356 Yagishita[51]. One unit of activity was defined as the enzymatic activity that produced 1 mmol
357 of GlcNAc per minute at 37°C.
358
359 *Antifungal activity assay*
360 *Qualitative assay*
361 An antifungal assay was performed according to the method of Schlumbaum *et al.*[17] with
362 modification. An agar disk (4 mm in diameter) containing the test fungus, *T. longibrachiatum*,
363 prepared from the cultured fungus on potato dextrose broth with 1.5% (w/v) agar (PDA), was
364 placed in the center of a Petri dish containing PDA. Wells were subsequently punched into the
365 agar at a 15 mm distance from the center of the Petri dish. 500 pmol of each protein sample
366 was placed into the wells. The plates were incubated for 24 hours at 25°C.
367 *Quantitative assay*
368 Hyphal re-extension inhibition assay was done by using *T. longibrachiatum*. Agar disks (4 mm
369 and 1 mm in diameter and in-depth, respectively) containing the fungal hyphae, which were
370 derived from the resting part of the fungus previously cultured on potato dextrose broth
371 containing 1.5% (w/v) agar (PDA), were put on another PDA plate with the hyphae attached
372 side down. Five μL of sterile water or sample solution were overlaid on the agar disks, and

373 then the plate was incubated at 25 °C for 12 hours. After incubation, images of the plates were
374 scanned using an image scanner. The areas of the re-extended hyphae were calculated as
375 numbers of pixels by GNU Image Manipulation Program (GIMP, ver. 2.0). The protein
376 concentration required for inhibiting the growth of the fungus by 50% was defined as IC_{50} and
377 determined by constructing dose-response curves (percentage of growth inhibition versus
378 protein concentration).
379
380 *Cell wall binding assay*
381 The binding activity of protein to the fungal cell wall was measured by pull down assay
382 followed by a previous method with modifications (ref). 5 μL of 10^6 spores/mL of
383 T.*longibrachiatum* was added to 1L of sterilized PDB (Potato dextrose broth) in a 3 L flask
384 and was incubated at 30°C for 48 h with shaking at 300 rpm to obtain the mycelia of the fungi.
385 The mycelia were collected by filtration, washed extensively with water and lyophilized. 1.5
386 g of the dried mycelia were incubated three times in 50 mL of 1M NaOH at 65°C for 30 min.
387 The alkali-insoluble pellet was washed five times with water and twice with 10 mM of sodium
388 acetate buffer (pH5.0) and lyophilized and stored as cell wall fraction.
389 250 μL of 0.2%(w/v) cell wall fraction suspension prepared in 10 mM sodium acetate buffer
390 (pH 5.0) was mixed with an equal volume of the protein solution. The mixture was incubated
391 at 25 and shaked with 1000 rpm for 1 hour. After shaking, the reaction mixture was centrifuged
392 at 12,000g for 20 min. The protein concentrations of the supernatant were measured with the
393 absorbance at 280 nm. The K_d and B_{max} (μmol/g of cell wall fraction) were determined by
394 fitting the binding isotherms to a one-site binding equation, where P represents protein; $[P_{bound}]$
395 $= B_{max} [P_{free}]/(K_d + [P_{free}])$. The fitting was done via nonlinear regression analysis.
396
397 *Differential scanning fluorimetry*

398 Differential scanning fluorimetry (DSF) experiments were performed using StepOnePlus
399 Instrument, a real-time PCR equipment. Reaction mixtures contained 2.5 μM protein in 10 mM
400 sodium acetate buffer, pH 5.0, 5× SYPRO orange dye in a total volume of 20 μL and dispensed
401 into a 96-well PCR plate. Fluorescence intensities were monitored continuously as the sample
402 mixtures were heated from 20 °C to 99 °C at a rate of 1% (approximately 1.33 °C/min), using
403 the ROX channel. Melting temperatures were determined by fitting the fluorescence derivative
404 data to a quadratic equation in the vicinity of the Tm in R software.
405
406 *Crystallization.*
407 After purification, Anc4 and Anc5 were concentrated at 10.0 mg/ml and 5.67 mg/ml in the 5
408 mM Tris-HCl buffer, pH 8.0, respectively. Anc4 + Loop II + A and Anc4 + Loop II + A+B+C
409 were concentrated at 6.00 mg/ml and 3.80 mg/ml in the 10 mM sodium acetate buffer
410 containing 150 mM NaCl, pH 5.0, respectively. Initial crystallization screens were performed
411 using various crystallization screening kits commercially available. The protein solution drop
412 (400 nL) was mixed with 400 nL of a reservoir solution and then equilibrated with 50 μL of
413 the reservoir solution using a crystallization robot, Mosquito® Xtal3. The crystallization
414 conditions were screened using the sparse-matrix sampling method, according to the sitting-
415 drop vapor diffusion method at 20 °C in a 96-well plate (violamo). After a week, well-formed
416 crystals of Anc4 and Anc5 were obtained using PEGRx 1 (Hampton Research) and further
417 optimized to the condition (15% and 27% (w/v) polyethylene glycol monomethyl ether 2,000,
418 0.1 M MES monohydrate pH 6.0 for Anc4 and Anc5, respectively). Well-formed crystals of
419 Anc4 + Loop II + A and Anc4 + Loop II + A+B+C were obtained using Eco-screen (Molecular
420 Dimensions) at the condition (25% (w/v) polyethylene glycol 3,350, 0.1 M Bis-Tris, pH 6.5).
421
422

423 *X-ray data collection*

424 For data collection, the crystals of Anc4 and Anc5 were soaked in cryoprotectant buffer (40%
425 (w/v) polyethylene glycol monomethyl ether 2,000, 0.1 M MES monohydrate pH 6.0) for 1
426 min before flash-cooling to 100K in liquid nitrogen. Diffraction datasets were collected at 100
427 K on BL32XU or BL41XU or BL45XU beamline of the SPring-8 (Harima, Japan), employing
428 the automated data collection ZOO[52]. The collected datasets were processed automatically with
429 KAMO[53]. Each dataset was indexed and integrated using XDS[54], followed by a hierarchical
430 clustering analysis using the correlation coefficients of the normalized structure amplitudes
431 between datasets. Finally, a group of outlier-rejected datasets was scaled and merged using
432 XSCALE[55] or Aimless[56].

433

434 *Structure solution and refinement*

435 General data handling was performed with the Phenix package[57]. The initial model was solved
436 by molecular replacement using Phaser[58] with the model structure of Anc4 and Anc5 predicted
437 by AlphaFold2[59] . The model building was performed with *Coot*[60]. Structures were refined by
438 *Coot*[60] and Phaser[58]. The details of crystallization, structure determination, the data collection,
439 data processing, and refinement statistics are given in Supplementary Tables 2 and 3. Structural
440 figures are described and rendered by the PyMOL Molecular Graphics System, Version
441 1.2r3pre, Schrödinger, LLC.

442

443 *Molecular Dynamics Simulations*

444 The MD simulations were performed using GROMACS version 2020.1[61] and the charmm36-
445 mar2019 force field[62]. The model structures were built using Anc4 and Anc5 structures
446 obtained from this work and used as a starting point for MD simulations. For each model, the
447 system was solvated and neutralized with Na^+ and Cl^- ions in a dodecahedral box. Temperature

448 was maintained at 310 K by using a modified Berendsen thermostat[63] and pressure was
449 maintained at 1 bar by using a Parrinello-Rahman barostat[64]. The system was then equilibrated
450 on energy, temperature, and pressure before performing four individual repeats of 200 ns of
451 the simulations. To analyze the fluctuation, Gromacs standard analysis package was used.
452

453 *Rigidity-based allosteric communication and FIRST*

454 Allostery analysis was carried out by applying rigidity-transmission allostery (RTA) analysis[24] .
455 The RTA method utilizes graph and rigidity theory[25,26] techniques to identify allosteric
456 networks within structures of proteins and protein complexes[27–30]. Starting with protein
457 structures of Anc4 + Loop II and Anc5ΔLoopI, we applied the RTA algorithm by sequentially
458 perturbing rigidity of individual residues and monitoring changes in conformational degrees of
459 freedom in loop II. Rigid cluster decomposition and dilution plots on Anc4 + Loop II and
460 Anc5ΔLoopI were performed with software FIRST[31]. FIRST creates a geometric molecular
461 framework, whose underlying network (graph) contains atoms (vertices) and edges (*i.e.*
462 constraints representing covalent bonds, hydrogen bonds, electrostatic interactions, and
463 hydrophobic contacts). Every potential hydrogen bond is assigned an energy strength in
464 kcal/mol, and a hydrogen bond cutoff energy value was selected so that all bonds weaker than
465 this cutoff are removed from the network. FIRST then applies the pebble game algorithm[26,65]
466 which rapidly decomposes a protein structure into flexible and rigid regions while
467 incrementally removing weak hydrogen bonds.

468 *Microscopic observations*

469 The catalytically inactive mutants of Anc4, Anc4 + Loop I, Anc5, AncΔ5 were tagged with
470 Alexa Fluor 488 Microscale Protein Labeling Kit (Thermo Fisher), followed by the
471 manufacturer's protocol.

472 The Alexa Fluor 488 reactive dye has a tetrafluorophenyl ester moiety that reacts with primary
473 amines of proteins to form conjugates.
474 10 mL of sterilized PDB (Potato dextrose broth) medium containing 10^6 spores/mL of T.
475 *longibrachiatum* was incubated at 25°C for 24 h with shaking at 300 rpm to obtain the mycelia
476 of the fungi. The mycelia were collected by centrifugation (3000*g*, 25 °C, 20 min) and was
477 resuspended by PDB medium. Then, 50 μL of the mycelial suspension was mixed with 50 μL
478 of 2 μM each protein sample solution and incubated at 25 °C for 1 h. The incubated solution
479 mixture was washed three times with 20 mM sodium phosphate buffer (pH 7.4). The samples
480 were observed with confocal laser scanning microscopy.

481

482 **Figures**

483

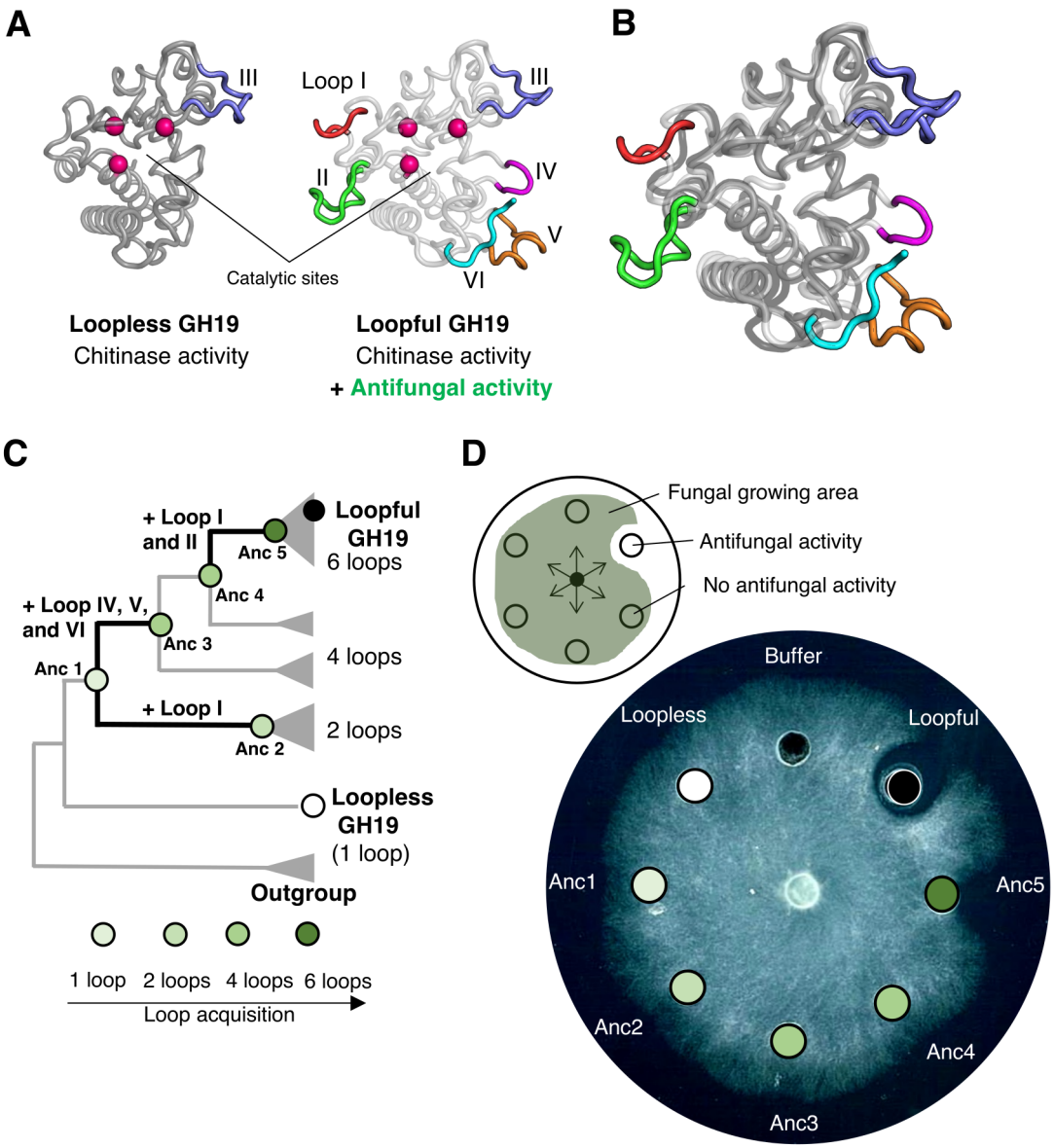

484

485 **Fig. 1. Antifungal activity is acquired during evolution in GH19 chitinase. A)** Structural
486 comparison of two types of GH19 chitinase, loopless and loopful. They share the core region
487 (darker and lighter grey in loopless and loopful GH19, respectively), two catalytic glutamic
488 acids, and one serine that holds catalytic water (magenta spheres) but differs in loop regions,
489 named I to VI. (shown in red, green, light blue, purple, orange, and cyan, respectively). B)
490 Structural superimposition of loopless and loopful. The detail catalytic mechanism that they
491 conserve is shown in Fig. S1. **C**) Schematic representation of a phylogenetic tree of GH19
492 chitinase. The five ancestral nodes that were characterized are labeled and colored according
493 to the number of loop regions (80% lighter green, one loop; 60% lighter green, two loops; 40%

494 lighter green, four loops; 25% darker green, six loops). Evolutionary transitions containing
495 loop acquisitions are highlighted with thick black lines. A multiple sequence alignment of two
496 modern and five ancestor sequences and a full phylogenetic tree are shown in Figs. S2 and S3,
497 respectively. **D)** Top, a schematic representation of fungal hyphae expansion inhibition assay
498 against *Trichoderma longibrachiatum* as the test fungus. Bottom, the assay plate. Each well
499 contains 10 μL of sterilized buffer (10 mM sodium acetate buffer, pH 5.0) or 500 pmol of
500 protein samples dissolved in the same buffer.

A

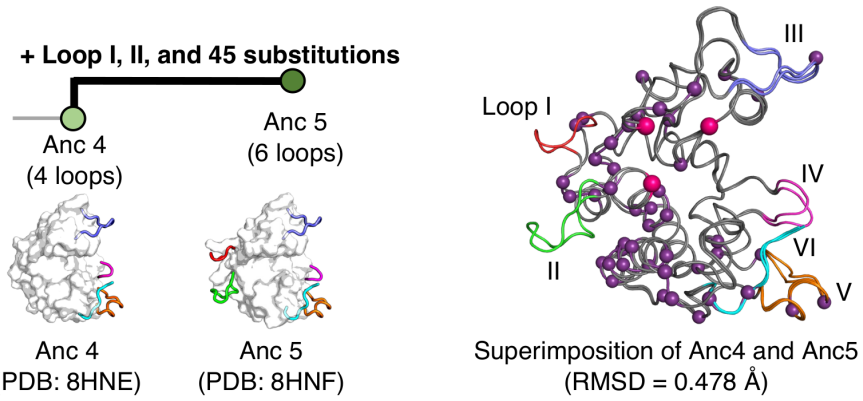

B

Variants	Chitinase activity (U/mol) $\times 10^9$	Antifungal activity (IC_{50}, μM)	Thermostability (Tm, °C)
Anc 4	1.05	488 ± 3	72.5
Anc 4 + Loop I	N. D.	N. D.	64.0
Anc 4 + Loop II	1.15	737 ± 7	64.0
Anc 4 + Loop I and II	N. D.	N. D.	55.0
Anc 5	0.85	16.9 ± 1.4	66.0
Anc 5 Δ Loop I	1.28	17.2 ± 1.9	60.0
Anc 5 Δ Loop II	1.04	200 ± 20	62.0
Anc 5 Δ Loop I and II	1.28	575 ± 4	72.0

C

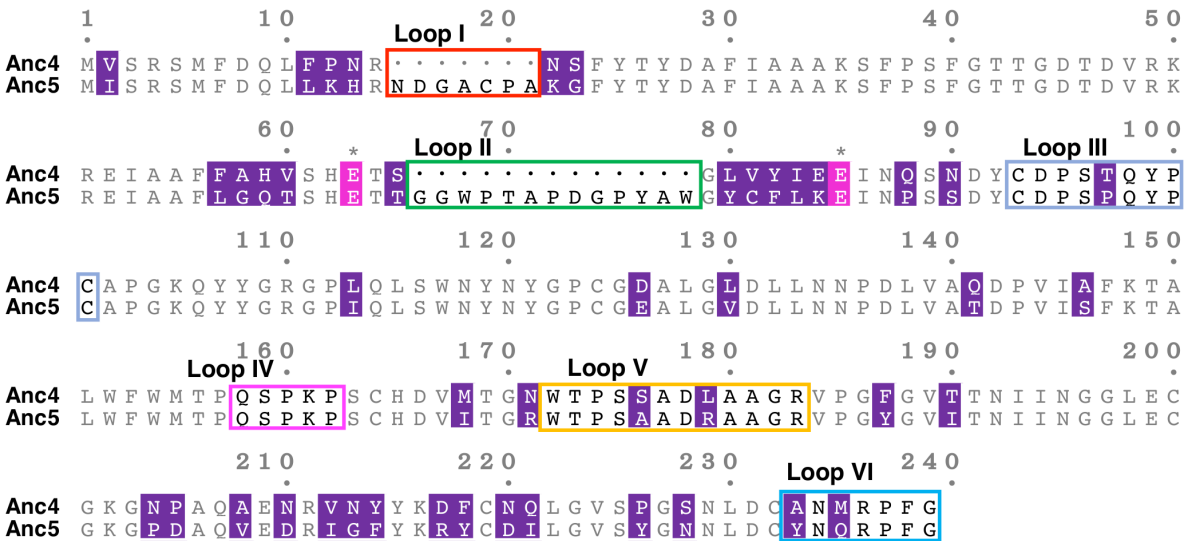

Fig. 2. Characterization of eight variants of two ancestral proteins reveal the key remote loop for the acquisition of antifungal activity. A) Left, a schematic representation of an evolutionary transition from Anc4 to Anc5. Crystal structures of Anc4 and Anc5 solved to 1.13

505 Å and 1.57 Å, respectively. Right, structural superimposition of Anc4 and Anc5. Two catalytic
506 glutamic acids and one serine reside that holds catalytic water are indicated as magenta spheres.
507 45 substitution residues are indicated as purple spheres. **B**) Summary of the effects of loop
508 presence/absence on the hydrolytic and antifungal activities. One unit of activity is defined as
509 the enzyme activity that produced one μmol of GlcNAc per minute at 37°C. Error bars
510 represent SD (n = 3). Melting temperature (T_m) was measured using differential scanning
511 fluorimetry followed by the procedures as described in the Methods. **C**) An alignment of Anc4
512 + Loop II and Anc5ΔLoop I sequence. Loop regions II to VI are highlighted in green, light
513 blue, purple, orange, and cyan squares, respectively. Two glutamate residues and one serine
514 residue are shown in magenta. 45 substitutions residues are shown in purple.

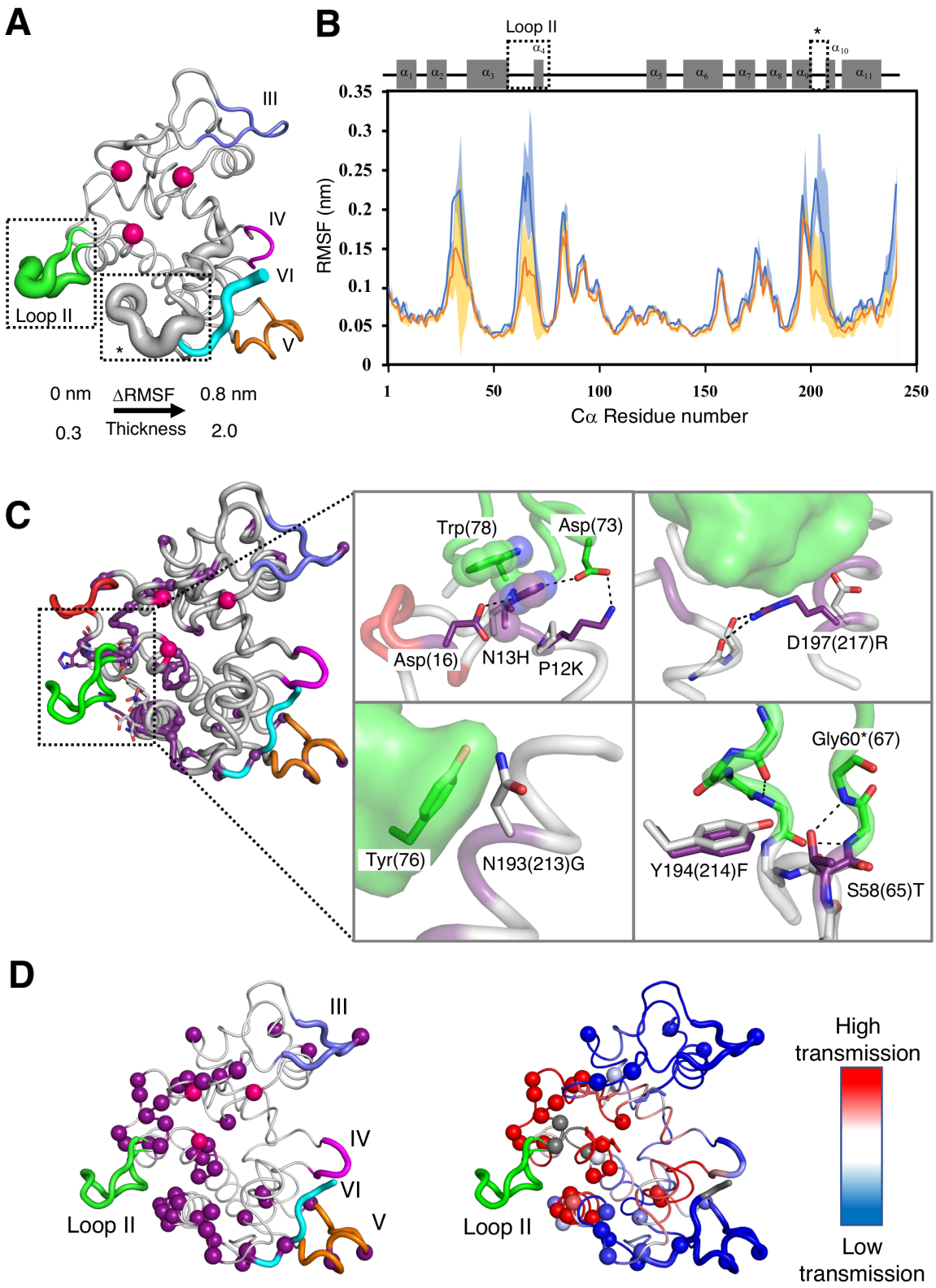

Fig. 3. Comparison of Anc4 + Loop II and Anc5ΔLoop I exhibit the structural and dynamics contribution of Loop II and scaffold substitutions. A) The difference in Δroot

518 mean square fluctuation (ΔRSMF = RMSF of Anc4 + Loop II – RMSF of Anc5ΔLoop I) is
519 mapped on the structure of Anc5ΔLoop I as the thickness of the cartoon representation. Spheres
520 indicates two catalytic glutamic acids and one serine that holds catalytic water. **B**) Plots of the
521 RMSF of Cα of each residue in Anc4 + Loop II (blue) and Anc5ΔLoop I (orange). Error bars
522 are indicated as shades. A schematic representation of secondary structures of GH19 chitinase
523 is shown. Dashed squares indicate the region where ΔRSMF is more than 0.05 nm. RMSDs of
524 the Cα atoms of all residues are shown in Fig. S5B. **C**) Cartoon_tube representation of Anc5.
525 Sphere representation indicates 45 substitution residues (purple) and two catalytic glutamic
526 acids and one serine that holds catalytic water (magenta). Resides around 4 Å from loop II are
527 shown in sticks. Intra molecular interactions stabilizing loop II regions are shown in the
528 enlargements. Resides in Anc4 and Anc5 state are shown in grey and purple sticks, respectively.
529 Black dashed lines indicate hydrogen bonds. Residue numbers are based on Anc4. In the case
530 that the number shifts due to loop insertions, residue numbers of Anc5 state are in parentheses.
531 An asterisk indicates the number of Anc4 + Loop II. Loop regions I to VI are shown in red,
532 green, light blue, purple, orange, and cyan, respectively. **D**) Left, computational analysis of
533 long-range communication in Anc5ΔLoop I. Cartoon representation of Anc5 ΔLoop I with
534 cartoon_tube representation of loop II to VI (shown in green, slate, purple, orange, and cyan,
535 respectively). Sphere representation indicates 45 substitutions residues (purple) and two
536 glutamic acids and one serine that holds catalytic water (magenta). Right, rigidity transmission
537 allostery (RTA) communication analysis on Anc5ΔLoop I. Residues are colored based on the
538 intensity (red being highest) of long-range rigidity transmission communication with loop II
539 (green). Spheres indicate 45 substitutions.
540
541

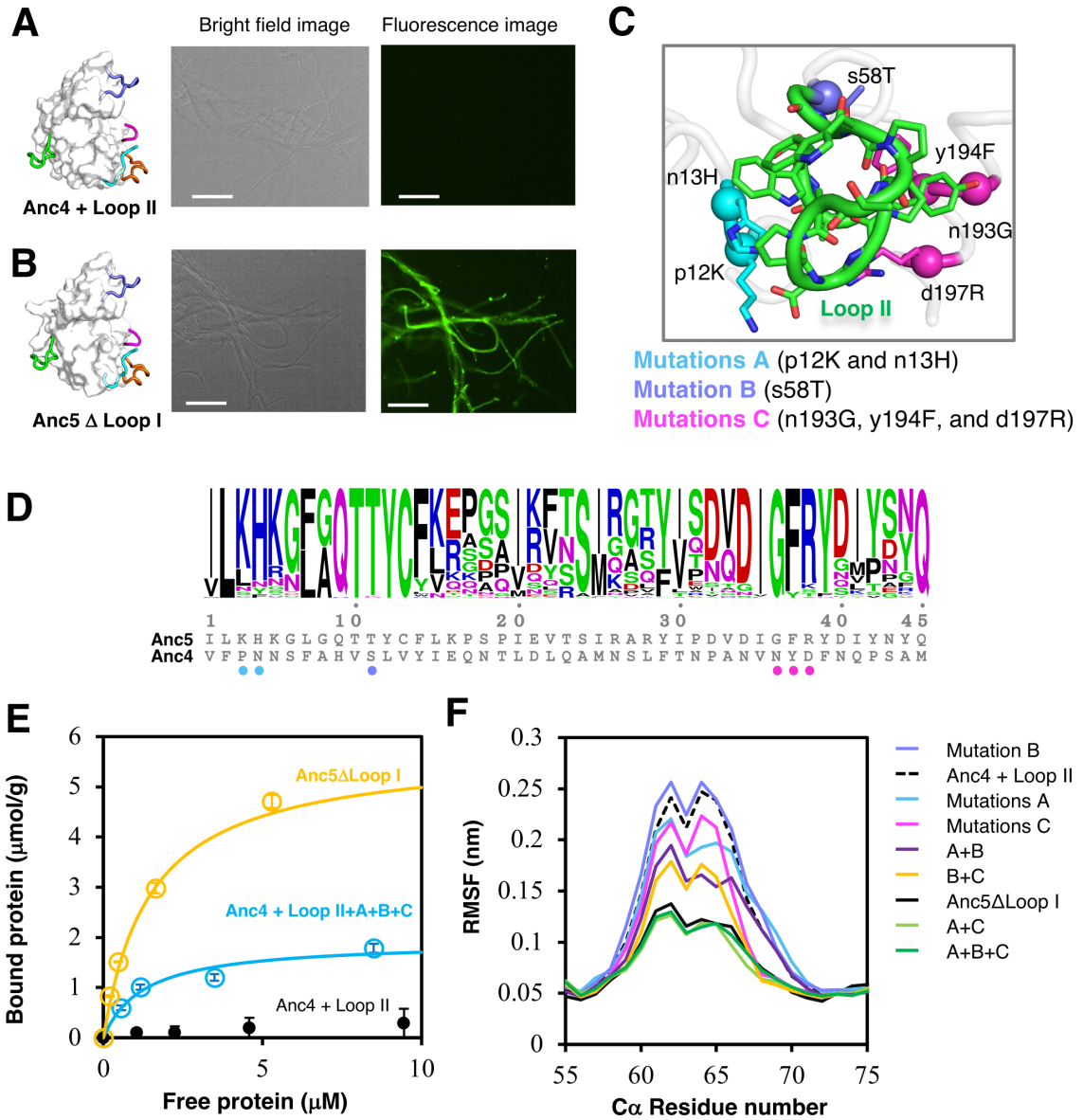

Fig. 4. Gain of antifungal activity through substitutions that rigidify loop II to bind fungal cell wall.

Each 50 μL of 2 μM Alexa Fluor 488-labelled proteins Anc4 + Loop II and Anc5ΔLoop I is mixed with *T. longibrachiatum* hyphae in 20 mM sodium phosphate buffer, pH 7.4 at 25 °C. Images were captured after washing excess of the labelled proteins. All scale bares are 100 μm. A) From left to right: the structure of Anc4 + Loop II; Bright field image of fungal hyphae; Fluorescence microscope image shows no binding to the surface of fungal hyphae. B) From left to right: the structure of Anc5ΔLoop I; Bright field image of fungal hyphae; Fluorescence

551 microscope image shows Alexa Fluor 488-labelled Anc5ΔLoop I binding to the surface of
552 fungal hyphae. C) The crystal structure of Anc4 + Loop II integrated with all six substitutions
553 (p12K, n13H, s58T, n193G, y194F, and d197R) revealed the interactions of these residues with
554 loop II. Substitutions were introduced gradually due to the convenience experimentally as
555 mutations A (cyan), p12K and n13H; mutation B (slate), s58T mutations C (magenta), n193G,
556 y194F, and d197R. Small and large characters indicate the Anc4 and Anc5 states, respectively.
557 Side chains and Cα atoms of the introduced residues are shown as stick and speres, respectively.

558 D) Sequence logo of 45 positions where substitutions occurred between Anc4 and Anc5. The
559 hight of logo represents the frequency of amino acid residues at each position among loopful-
560 type GH19 chitinases. E) Binding curves of Anc4 + Loop II+A+B+C and Anc5ΔLoop I.
561 Binding curves were fitted with plots of the absorbance of the supernatants of each protein
562 samples at 280 nm after pulldown assay. The pulldown assay was performed in 10 mM sodium
563 acetate buffer (pH 5.0) at 25°C, using 0.1% (w/v) cell wall fraction from T. *longibrachiatum*
564 as the substrate. F) RMSFs of the Cα atoms of Loop II residues in Anc4 + Loop II, Anc5ΔLoop
565 I, and mutants of Anc4 + Loop II. RMSDs of the Cα atoms of all residues are shown in Fig.
566 S5B.

567

568 **Table 1 Enzymatic activities and melting temperature of the two modern and five ancestral GH19**
569 **chitinases**

Protein	Loop	Specific activity (U*/mol) × 10^9	DSF T_m (°C)
Anc1	III	1.44	58.5
Anc2	I and III	0.75	52.0
Anc3	III, IV, V, and VI	1.20	72.0
Anc4	III, IV, V, and VI	1.05	72.5
Anc5	I, II, III, IV, V, and VI	0.85	66.0
Loopless	III	1.51	68.0
Loopful	I, II, III, IV, V, and VI	0.83	62.5

570 * One unit of activity is defined as the enzyme activity that produced one μmol of GlcNAc per
571 minute at 37° C. Melting temperature (T_m) was measured using differential scanning
572 fluorimetry (DSF) followed by the procedures as described in the Methods.
573
574
575
576
577
578
579
580
581
582
583

584 **Table 2 Summary of enzymatic and binding parameters of Anc4 + Loop II, its mutants,**

585 **and Anc5ΔLoop I**

Variants	Mutations	Hydrolytic activity (U*/mol) ×10^9	Antifungal activity (IC50)	Binding activity *B*max (μmol/g)	*K*d (μM)
Anc4 + II	N/A	1.15	737 ± 7	0.57 ± 0.20	8.93 ± 5.46
Anc4 + II +A	n13H/p12K	1.09	155.9 ± 13	n.d	n.d
Anc4 + II +B	s58T	1.14	593 ± 22	n.d	n.d
Anc4 + II +C	d197R/y194F/d197R	1.32	136.2 ± 4.3	1.66 ± 0.61	4.31 ± 2.06
Anc4 + II +A+B		0.79	129.3 ± 5.7	n.d	n.d
Anc4 + II +A+C		1.44	128.8 ± 7.4	3.61 ± 0.29	3.33 ± 0.71
Anc4 + II +B+C		1.43	72.6 ± 10	0.76 ± 0.29	1.75 ± 0.33
Anc4 + II +A+B+C		1.43	63.43 ± 3.8	2.04 ± 0.04	1.59 ± 0.07
Anc5 Δ I	45 subs	1.28	17.2 ± 1.9	5.93 ± 0.19	1.47 ± 0.11

586

587 **Acknowledgments**

588 Financial support by Okinawa Institute of Science and Technology (OIST) is gratefully

589 acknowledged. We thank Nobuhiko Tokuriki for the discussion on the project. We thank Toki

590 Taira, and Ben Clifton and Erika Fukuhara for their insightful comments on this manuscript.

We are grateful for the help provided by the scientific computing, the Data Analysis, and the Instrumental sections at OIST. We also thank Paolo Barzaghi from the Imaging Section of OIST for the help with microscope experiments and Stefano Pascarelli for assistance with molecular dynamics simulations. The synchrotron radiation experiments were performed at BL45XU and BL41XU of SPring-8 with the approval of the Japan Synchrotron Radiation Research Institute (JASRI) (Proposal No. 2022A2769)

Author contributions

D.K. and P.L. designed the project. D.K. performed phylogenetic analysis, all the biochemical experiments, biophysical characterization of all the proteins and mutants, fluorescent imaging microscope experiments, and molecular dynamics simulations. A.S. performed rigidity-transmission allostery computation and the related data analysis. D.K. and P.L. wrote the manuscript with the input from A.S. This project was supervised by P.L.

605 **References**

606
607
608
609

610 1. Arnold, F. H. Innovation by evolution: bringing new chemistry to life (nobel lecture).
611 *Angew. Chem. Int. Ed* **58**, 14420–14426 (2019).

612 2. Tawfik, D. S. Biochemistry. Loop grafting and the origins of enzyme species. *Science*
613 **311**, 475–476 (2006).

614 3. Burroughs, A. M., Allen, K. N., Dunaway-Mariano, D. & Aravind, L. Evolutionary
615 genomics of the HAD superfamily: understanding the structural adaptations and
616 catalytic diversity in a superfamily of phosphoesterases and allied enzymes. *J. Mol.*
617 *Biol.* **361**, 1003–1034 (2006).

618 4. Akiva, E., Copp, J. N., Tokuriki, N. & Babbitt, P. C. Evolutionary and molecular
619 foundations of multiple contemporary functions of the nitroreductase superfamily.
620 *Proc Natl Acad Sci USA* **114**, E9549–E9558 (2017).

621 5. Monzingo, A. F., Marcotte, E. M., Hart, P. J. & Robertus, J. D. Chitinases,
622 chitosanases, and lysozymes can be divided into procaryotic and eucaryotic families
623 sharing a conserved core. *Nat. Struct. Biol.* **3**, 133–140 (1996).

624 6. Park, H.-S. *et al.* Design and evolution of new catalytic activity with an existing
625 protein scaffold. *Science* **311**, 535–538 (2006).

626 7. Afriat-Jurnou, L., Jackson, C. J. & Tawfik, D. S. Reconstructing a missing link in the
627 evolution of a recently diverged phosphotriesterase by active-site loop remodeling.
628 *Biochemistry* **51**, 6047–6055 (2012).

629 8. Miton, C. M. & Tokuriki, N. Insertions and deletions (indels): A missing piece of the
630 protein engineering jigsaw. *Biochemistry* (2022) doi:10.1021/acs.biochem.2c00188.

631 9. Brejc, K. *et al.* Crystal structure of an ACh-binding protein reveals the ligand-binding
632 domain of nicotinic receptors. *Nature* **411**, 269–276 (2001).

633 10. Huse, M. & Kuriyan, J. The conformational plasticity of protein kinases. *Cell* **109**,
634 275–282 (2002).

635 11. Fushinobu, S., Nishimasu, H., Hattori, D., Song, H.-J. & Wakagi, T. Structural basis
636 for the bifunctionality of fructose-1,6-bisphosphate aldolase/phosphatase. *Nature* **478**,
637 538–541 (2011).

638 12. Hoque, M. A. *et al.* Stepwise loop insertion strategy for active site remodeling to
639 generate novel enzyme functions. *ACS Chem. Biol.* **12**, 1188–1193 (2017).

640 13. Dodani, S. C. *et al.* Discovery of a regioselectivity switch in nitrating P450s guided
641 by molecular dynamics simulations and Markov models. *Nat. Chem.* **8**, 419–425
642 (2016).

643 14. Hedstrom, L., Szilagyi, L. & Rutter, W. J. Converting trypsin to chymotrypsin: the
644 role of surface loops. *Science* **255**, 1249–1253 (1992).

645 15. Ma, W., Tang, C. & Lai, L. Specificity of trypsin and chymotrypsin: loop-motion-
646 controlled dynamic correlation as a determinant. *Biophys. J.* **89**, 1183–1193 (2005).

647 16. Gunasekaran, K., Ma, B. & Nussinov, R. Triggering loops and enzyme function:
648 identification of loops that trigger and modulate movements. *J. Mol. Biol.* **332**, 143–
649 159 (2003).

650 17. Schlumbaum, A., Mauch, F., Vögeli, U. & Boller, T. Plant chitinases are potent
651 inhibitors of fungal growth. *Nature* **324**, 365–367 (1986).

652 18. Taira, T. *et al.* Cloning and characterization of a small family 19 chitinase from moss
653 (Bryum coronatum). *Glycobiology* **21**, 644–654 (2011).

654 19. Fukamizo, T. *et al.* A flexible loop controlling the enzymatic activity and specificity
655 in a glycosyl hydrolase family 19 endochitinase from barley seeds (Hordeum vulgare
656 L.). *Biochim. Biophys. Acta* **1794**, 1159–1167 (2009).

657 20. Tanaka, J., Fukamizo, T. & Ohnuma, T. Enzymatic properties of a GH19 chitinase
658 isolated from rice lacking a major loop structure involved in chitin binding.
659 *Glycobiology* **27**, 477–485 (2017).

660 21. Takenaka, S., Ohnuma, T. & Fukamizo, T. Insertion of a Loop Structure into the
661 "Loopless" GH19 Chitinase from Bryum coronatum. *J. Appl. Glycosci. (1999)* **64**,
662 39–42 (2017).

663 22. Kawamoto, D., Takashima, T., Fukamizo, T., Numata, T. & Ohnuma, T. A conserved
664 loop structure of GH19 chitinases assists the enzyme function from behind the core-
665 functional region. *Glycobiology* **32**, 356–364 (2022).

666 23. Mizuno, R. *et al.* Role of the loop structure of the catalytic domain in rice class I
667 chitinase. *J. Biochem.* **143**, 487–495 (2008).

668 24. Sljoka, A. Probing Allosteric Mechanism with Long-Range Rigidity Transmission
669 Across Protein Networks. *Methods Mol. Biol.* **2253**, 61–75 (2021).

670 25. Whiteley, W. Counting out to the flexibility of molecules. *Phys. Biol.* **2**, S116-26
671 (2005).

672 26. Sljoka, A. Structural and functional analysis of proteins using rigidity theory. in
673 *Sublinear computation paradigm: algorithmic revolution in the big data era* (eds.
674 Katoh, N. et al.) 337–367 (Springer Singapore, 2022). doi:10.1007/978-981-16-4095-
675 7_14.

676 27. Huang, S. K. *et al.* Delineating the conformational landscape of the adenosine A2A
677 receptor during G protein coupling. *Cell* **184**, 1884-1894.e14 (2021).

678 28. Mehrabi, P. *et al.* Substrate-Based Allosteric Regulation of a Homodimeric Enzyme.
679 *J. Am. Chem. Soc.* **141**, 11540–11556 (2019).

680 29. Baksh, K. A., Augustine, J., Sljoka, A., Prosser, R. S. & Zamble, D. B. Mechanistic
681 insights into the nickel-dependent allosteric response of the Helicobacter pylori NikR
682 transcription factor. *J. Biol. Chem.* 102785 (2022) doi:10.1016/j.jbc.2022.102785.

683 30. Ye, L. *et al.* Mechanistic insights into allosteric regulation of the A2A adenosine G
684 protein-coupled receptor by physiological cations. *Nat. Commun.* **9**, 1372 (2018).

685 31. Jacobs, D. J., Rader, A. J., Kuhn, L. A. & Thorpe, M. F. Protein flexibility predictions
686 using graph theory. *Proteins* **44**, 150–165 (2001).

687 32. Yamagami, T. & Funatsu, G. Identification of the Tryptophan Residue Located at the
688 Substrate-binding Site of Rye Seed Chitinase-c. *Biosci. Biotechnol. Biochem.* **59**,
689 1076–1081 (1995).

690 33. Chothia, C., Gough, J., Vogel, C. & Teichmann, S. A. Evolution of the protein
691 repertoire. *Science* **300**, 1701–1703 (2003).

692 34. Rockah-Shmuel, L. *et al.* Correlated occurrence and bypass of frame-shifting
693 insertion-deletions (InDels) to give functional proteins. *PLoS Genet.* **9**, e1003882
694 (2013).

695 35. Emond, S. *et al.* Accessing unexplored regions of sequence space in directed enzyme
696 evolution via insertion/deletion mutagenesis. *Nat. Commun.* **11**, 3469 (2020).

697 36. Schenkmayerova, A. *et al.* Engineering the protein dynamics of an ancestral
698 luciferase. *Nat. Commun.* **12**, 3616 (2021).

699 37. Ross, C. M., Foley, G., Boden, M. & Gillam, E. M. J. Using the Evolutionary History
700 of Proteins to Engineer Insertion-Deletion Mutants from Robust, Ancestral Templates
701 Using Graphical Representation of Ancestral Sequence Predictions (GRASP).
702 *Methods Mol. Biol.* **2397**, 85–110 (2022).

703 38. Macdonald, C. B. *et al.* Deep insertion, deletion, and missense mutation libraries for
704 exploring protein variation in evolution, disease, and biology. *BioRxiv* (2022)
705 doi:10.1101/2022.07.26.501589.

706 39. Campbell, E. *et al.* The role of protein dynamics in the evolution of new enzyme
707 function. *Nat. Chem. Biol.* **12**, 944–950 (2016).

708 40. Liu, J., Tan, H. & Rost, B. Loopy proteins appear conserved in evolution. *J. Mol.*
709 *Biol.* **322**, 53–64 (2002).

710 41. Tóth-Petróczy, A. & Tawfik, D. S. Protein insertions and deletions enabled by neutral
711 roaming in sequence space. *Mol. Biol. Evol.* **30**, 761–771 (2013).

712 42. Tokuriki, N. *et al.* Diminishing returns and tradeoffs constrain the laboratory
713 optimization of an enzyme. *Nat. Commun.* **3**, 1257 (2012).

714 43. Noda-Garcia, L. & Tawfik, D. S. Enzyme evolution in natural products biosynthesis:
715 target- or diversity-oriented? *Curr. Opin. Chem. Biol.* **59**, 147–154 (2020).

716 44. Kaltenbach, M., Emond, S., Hollfelder, F. & Tokuriki, N. Functional Trade-Offs in
717 Promiscuous Enzymes Cannot Be Explained by Intrinsic Mutational Robustness of
718 the Native Activity. *PLoS Genet.* **12**, e1006305 (2016).

719 45. Arantes, V. & Saddler, J. N. Cellulose accessibility limits the effectiveness of
720 minimum cellulase loading on the efficient hydrolysis of pretreated lignocellulosic
721 substrates. *Biotechnol. Biofuels* **4**, 3 (2011).

722 46. UniProt Consortium. UniProt: the universal protein knowledgebase in 2021. *Nucleic*
723 *Acids Res.* **49**, D480–D489 (2021).

724 47. Katoh, K., Misawa, K., Kuma, K. & Miyata, T. MAFFT: a novel method for rapid
725 multiple sequence alignment based on fast Fourier transform. *Nucleic Acids Res.* **30**,
726 3059–3066 (2002).

727 48. Larsson, A. AliView: a fast and lightweight alignment viewer and editor for large
728 datasets. *Bioinformatics* **30**, 3276–3278 (2014).

729 49. Nguyen, L.-T., Schmidt, H. A., von Haeseler, A. & Minh, B. Q. IQ-TREE: a fast and
730 effective stochastic algorithm for estimating maximum-likelihood phylogenies. *Mol.*
731 *Biol. Evol.* **32**, 268–274 (2015).

732 50. Nozaki, S. & Niki, H. Exonuclease III (XthA) Enforces In Vivo DNA Cloning of
733 Escherichia coli To Create Cohesive Ends. *J. Bacteriol.* **201**, (2019).

734 51. Imoto, T. & Yagishita, K. A simple activity measurement of lysozyme. *Agric. Biol.*
735 *Chem.* **35**, 1154–1156 (1971).

736 52. Hirata, K. *et al.* ZOO: an automatic data-collection system for high-throughput
737 structure analysis in protein microcrystallography. *Acta Crystallogr. D Struct. Biol.*
738 **75**, 138–150 (2019).

739 53. Yamashita, K., Hirata, K. & Yamamoto, M. KAMO: towards automated data
740 processing for microcrystals. *Acta Crystallogr. D Struct. Biol.* **74**, 441–449 (2018).

741 54. Kabsch, W. *XDS*. in *International Tables for Crystallography: Crystallography of*
742 *biological macromolecules* (eds. Arnold, E., Himmel, D. M. & Rossmann, M. G.) vol.
743 F 304–310 (International Union of Crystallography, 2012).

744 55. Kabsch, W. Automatic processing of rotation diffraction data from crystals of initially
745 unknown symmetry and cell constants. *J. Appl. Crystallogr.* **26**, 795–800 (1993).

746 56. Winn, M. D. *et al.* Overview of the CCP4 suite and current developments. *Acta*
747 *Crystallogr. D Biol. Crystallogr.* **67**, 235–242 (2011).

748 57. Afonine, P. V. *et al.* Towards automated crystallographic structure refinement with
749 phenix.refine. *Acta Crystallogr. D Biol. Crystallogr.* **68**, 352–367 (2012).

750 58. McCoy, A. J. *et al.* Phaser crystallographic software. *J. Appl. Crystallogr.* **40**, 658–
751 674 (2007).

752 59. Jumper, J. *et al.* Highly accurate protein structure prediction with AlphaFold. *Nature*
753 **596**, 583–589 (2021).

754 60. Emsley, P. & Cowtan, K. Coot: model-building tools for molecular graphics. *Acta*
755 *Crystallogr. D Biol. Crystallogr.* **60**, 2126–2132 (2004).

756 61. Páll, S. *et al.* Heterogeneous parallelization and acceleration of molecular dynamics
757 simulations in GROMACS. *J. Chem. Phys.* **153**, 134110 (2020).

758 62. Huang, J. & MacKerell, A. D. CHARMM36 all-atom additive protein force field:
759 validation based on comparison to NMR data. *J. Comput. Chem.* **34**, 2135–2145
760 (2013).

761 63. Bussi, G., Donadio, D. & Parrinello, M. Canonical sampling through velocity
762 rescaling. *J. Chem. Phys.* **126**, 014101 (2007).

763 64. Parrinello, M. Polymorphic transitions in single crystals: A new molecular dynamics
764 method. *J. Appl. Phys.* **52**, 7182 (1981).

765 65. Jacobs, D. J. & Hendrickson, B. An Algorithm for Two-Dimensional Rigidity
766 Percolation: The Pebble Game. *J. Comput. Phys.* **137**, 346–365 (1997).